Solids velocity fields in a cold-flow gas-solid vortex reactor

Chemical Engineering Science 123 (2015) 220–230

Contents lists available at ScienceDirect

Chemical Engineering Science

journal homepage: www.elsevier.com/locate/ces

Solids velocity fields in a cold-flow Gas–Solid Vortex Reactor

Jelena Z. Kovacevic [a], Maria N. Pantzali [a], Kaustav Niyogi [a], Niels G. Deen [b], Geraldine J. Heynderickx [a,*], Guy B. Marin [a]

[a] Ghent University, Laboratory for Chemical Technology, Technologiepark 914, B-9052 Gent, Belgium
[b] Multiphase Reactors Group, Department of Chemical Engineering and Chemistry, Eindhoven University of Technology, P.O. Box 513, 5600 MB Eindhoven, The Netherlands

HIGHLIGHTS

- Velocity fields and velocity profiles in a Vortex Reactor are studied.
- Lower solids density or smaller diameter results in higher particle velocity.
- Higher solids density or smaller particle diameter reduces bubbling.
- A model to calculate particle velocity at the max solids capacity is proposed.

GRAPHICAL ABSTRACT

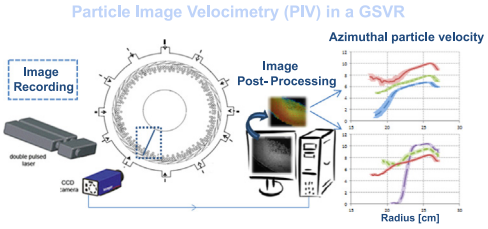

ARTICLE INFO

Article history:
Received 23 June 2014
Received in revised form
15 September 2014
Accepted 12 October 2014
Available online 24 October 2014

Keywords:
Gas–Solid Vortex Reactor
Fluidization
Bubbling
Particle velocity
PIV
Multiphase flow

ABSTRACT

In a Gas–Solid Vortex Reactor (GSVR), also referred to as a Rotating Fluidized Bed in Static Geometry, a fluidized bed is generated in a centrifugal field by introducing the gas via tangential inlet slots to the reactor chamber. Better heat and mass transfer are observed, making this a promising reactor type for Process Intensification. Developing GSVRs on industrial scale requires, amongst other, a good insight and understanding of the hydrodynamics of the granular flow. In the present work experiments are performed over a wide range of operating conditions in a cold flow pilot-scale set-up. The set-up has a diameter of 0.54 m, a length of 0.1 m and 36 tangential inlet slots of 2 mm. Different materials with solids density between 950–1800 kg/m^3 and particle diameters of 1–2 mm, at varying gas injection velocities from 55 to 110 m/s are tested between minimum and maximum solids capacities. All these operating conditions are used to follow the change of granular flow by performing PIV. The rotating fluidized bed can change from a smoothly rotating, densely fluidized bed to a highly bubbling rotating fluidized bed depending on the operating conditions. Bubbling diminishes with increasing solids density and particle diameter. Experimental measurements of azimuthal particle velocity fields in a GSVR are for the first time reported. Azimuthal solids velocity is found to decrease with higher solids density and larger particle diameter. The critical minimum fluidization velocity, that is the minimum velocity at which the complete bed is fluidized, is calculated and the centrifugal bed behavior is mapped in terms of a dimensionless radial gas velocity and a dimensionless particle diameter, as conventionally done for gravitational beds.

1. Introduction

Fluidization has been a topic of research for more than 60 years and different types of fluidization have been observed in conventional fluidized beds, depending on particle properties, particle diameter, solids density, fluid properties and fluid flow (Kunii and Levenspiel, 1969). Geldart (1973) classified particles in four groups (A, B, C, D) determined by the particle fluidization behavior in the gravitational field which depends on their mean particle size and the density difference between the particles and the fluidizing agent. Taking into account the particle classification by Geldart and the fluid properties

* Corresponding author: Tel.: +32 9 3311753; fax: +32 9 3311759.
E-mail address: Geraldine.Heynderickx@UGent.be (G.J. Heynderickx).

http://dx.doi.org/10.1016/j.ces.2014.10.020
0009-2509/

and flow rates Grace (1986) constructed a fluidization flow regime map for gravitational fluidization. Fluidized beds operating in a centrifugal field however can offer significant enhancement of heat and mass transfer due to improved gas–solid contact (Kovacevic et al., 2014), resulting in Process Intensification (PI). The concept of a Rotating Fluidized Bed (RFB) was proposed more than 30 years ago (Levy et al., 1979). A centrifugal field was generated by using a motor to make the reactor vessel rotate, while fluidization of the particle bed was realized by radial injection of gas through the side wall of the vessel. Kroger and Levy (1979) studied both packed and fluidized beds in a rotating vessel. In their experiments Kroger et al. (1980) visually observed that Geldart-B and Geldart-D particles give bubbling fluidization in a centrifugal field. Takahashi et al. (1984) and Fan et al. (1985) studied experimentally and analytically the bed pressure drop and minimum fluidization velocity in RFBs. The layer-by-layer fluidization theory developed by Chen (1987) and Kao et al. (1987) was experimentally confirmed by Qian et al. (1999) for Geldart-A particles. With increasing gas injection velocity, the bed is observed to evolve from a packed bed, to a partially fluidized bed and finally to a totally fluidized bed. When the bed is fully fluidized, bubbling behavior is reported by Qian et al. (1999). Shortly afterwards, Qian et al. (2001) showed that particles behave differently in the gravitational and in a centrifugal field. Particles observed to behave like Geldart-A particles in the gravitational field can shift to Geldart-B particle behavior in a centrifugal field. Correspondingly, Geldart-C particles shift to Geldart-A particle behavior. Nakamura and Watano (2007) experimentally and computationally reported that Geldart-B particle fluidization in a centrifugal field is bubbling in nature. Moreover, fluidization regimes in RFBs change from a fixed bed to a partially fluidized bed and to a partially bubbling bed, with increasing gas flow rate. When the gas flow rate is further increased the bubble distribution in the bed is observed to become uniform. Finally turbulent fluidization is reached. Even though the fluidization behavior of RFBs is quite extensively studied, particle velocities have not been reported, as particles are supposed to rotate with the velocity of the motor-driven rotating vessel.

An alternative approach to replace the gravitational by a centrifugal field was proposed with the design of a Gas–Solid Vortex Reactor (GSVR) (Anderson et al., 1972; De Wilde and de Broqueville, 2007, 2008; Dutta et al., 2010; Kochetov et al., 1969; Volchkov et al., 1993). No motor is used and the vessel is static. The gas is introduced in the reactor chamber, using tangential inlet slots, thus inducing tangential motion of the particles and making them rotate. Gas is continuously injected and leaves the reactor chamber through a central gas outlet. An overview of the advantages and disadvantages of the GSVR and RFB reactors over the conventional gravitational fluidized bed reactors was given by Kovacevic et al. (2014). Even though there are similarities in the flow pattern between the RFB and the GSVR, as they both comprise a rotating bed, there are also significant differences given that in the GSVR the walls are static and the air is tangentially introduced at considerably higher velocities to trigger particle rotation and fluidization. The literature available on the flow pattern characteristics in the GSVR is relatively limited. Studies of the fluidization pattern and the influence of various operating parameters are mostly qualitative. De Wilde and de Broqueville (2008) investigated the fluidization behavior of a bed of Geldart-B particles. At very low solids mass in the bed (solids capacity of the bed), channeling is observed, while with increase of mass, bubbling was found to be the main type of fluidization. For Geldart-D particles both channeling and slugging are observed at very low bed mass. With increasing solids capacity, a dense, stable and uniform bed is formed. Ekatpure et al. (2011) have experimentally studied the influence of the tangential slot thickness and the particle diameter on the bed behavior. The influence of particle diameter, particle density and gas injection velocity on the maximum solids capacity and the stability of the rotating bed was investigated by Kovacevic et al. (2014). Eliaers et al. (2014) showed experimentally that Geldart-C particles, which are difficult to fluidize under gravitational conditions, can be fluidized in a GSVR presenting Geldart-A particle behavior, as suggested by Qian et al. (2001) for RFBs. Detailed velocity data are lacking in literature. Anderson et al. (1972) measured the average flow velocity at different radii and reported a significant reduction of the angular flow velocity with increasing bed mass. This observation becomes more prominent at radii close to the end-walls. Dvornikov and Belousov (2011) measured some average particle velocities at two axial heights and reported that the particle velocity close to the wall is lower than in the center of the GSVR. Contrary to the RFBs, where the motor rotation (determining the azimuthal gas and particle velocity) and the gas injection velocity (determining the radial gas velocity) are independent, the tangentially injected gas makes the particles rotate and fluidizes the bed in GSVR. Azimuthal and radial particle velocity cannot be imposed independently. Experimental data for detailed particle velocity profiles developed in a GSVR which are of major importance to gain insight in the flow behavior of the GSVR have not been reported in literature. They are however required to optimize the GSVR geometry and operating conditions. Furthermore, validation of analytical models or numerical simulations also requires accurate experimental data. The present work determines the influence of particle diameter, particle density and gas injection velocity on the azimuthal particle velocity, as well as on the bed behavior in a cold flow GSVR pilot set-up. The experiments are performed using three materials and three particle diameters at four azimuthal gas injection velocities and with solids capacities up to the maximum capacity that can be set without particle entrainment.

2. Experimental set-up and procedure

2.1. Experimental set-up

The GSVR experimental set-up used in the present study is described in detail by Ekatpure et al. (2011) and by Kovacevic et al. (2014). A schematic diagram of the whole set-up is shown in Fig. 1(a), while the reactor main chamber is shown schematically in Fig. 1(b).

A two velocity component so called 2D Standard Particle Image Velocimetry (PIV) set-up (LaVision®) with a CCD camera of 4MP (Imager ProX4M) and a YAG Litron laser of 135 mJ is used to monitor the behavior of the rotating bed and to measure the azimuthal and radial particle velocities.

PIV is an optical method widely used in literature for studying fluidized bed flows (e.g. van Buijtenen et al., 2011). Typically PIV is used to obtain planar flow velocity fields by illuminating small (<20 microns) tracer particles following the fluid motion, with camera images having 2–3 pixels per particle. In the present study, a 2D PIV is used to measure the velocity of 1–2 mm diameter particles based on camera images having 10–40 pixels per particle. The particles used are not tracers and hence the particle velocity field will not match the fluid velocity field. The displacement of the particles and the time between two consecutive images is used to calculate the particle velocity and to obtain a 2D particle velocity vector field of the particulate flow.

Typically, in 2D PIV, particles in a fluid flow are illuminated twice, with a small time separation, by using a light sheet that is formed by passing a double pulsed laser beam through an optical arrangement including cylindrical lenses. In the present study, an evenly diffused laser light is used, instead of the light sheet. The corresponding measuring plane, near the rear end wall, is obtained with fully opened camera shutter aperture, limiting the measuring depth of the field of view. In particle free flow the total

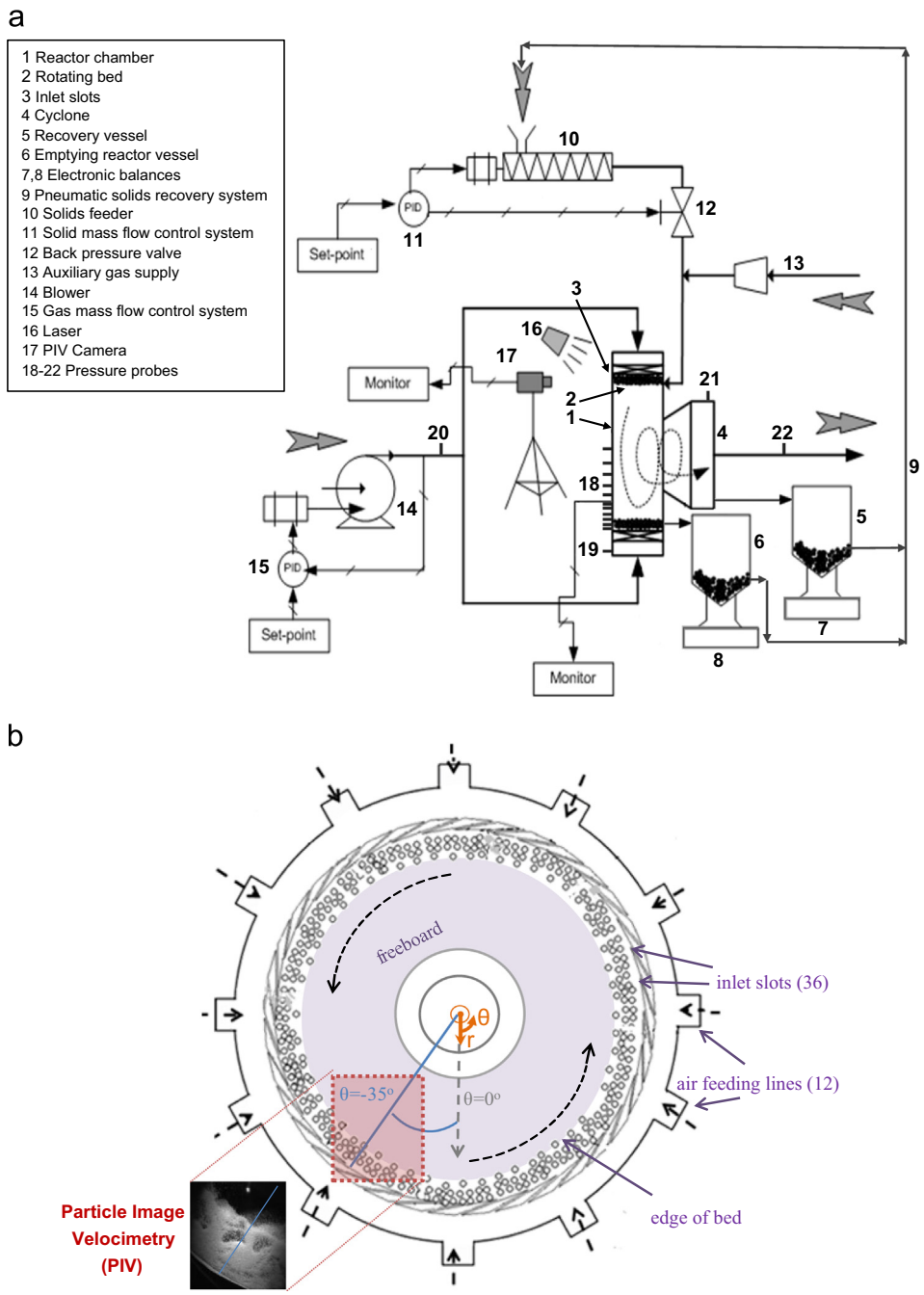

Fig. 1. (a) Schematic diagram of the GSVR set-up. (b) Detailed representation of the GSVR main chamber and jacket with 12 feeding lines and 36 inlet slots. The PIV recording window of 12×12 cm^2 is indicated by the dotted line.

depth of view is 9–14 mm. The presented fields correspond to images of the order of 12×12 cm^2. The area where PIV images are recorded and consequently particle velocities are measured is surrounded by a dotted line in Fig. 1(b). Averaged particle velocities presented in the paper are calculated at the indicated azimuthal angle ($\theta = -35^\circ$).

DaVis software by LaVision® is used for synchronizing the camera and laser pulses used to illuminate the particles, and for recording the images. The time between two laser pulses can be as small as 200 ns. Thus pairs of images of the rotating bed in the GSVR are captured with a high frequency. An appropriate time separation between two PIV frames is mostly determined by a minimum value desired for the displacement of particles between the two images. As a general guideline, literature recommends to limit the particle displacement to one quarter of the final interrogation window size (Keane and Adrian, 1990). In the present study this value is determined to be 8 pixels, as 32×32 interrogation windows are used as final interrogation windows for most experiments. It is experimentally verified that a further increase of the number of pixels no longer affected the values of the measured particle velocities. For the largest particles, larger interrogation windows are used, but an 8-pixel displacement is proven adequate to obtain reliable PIV vector fields. Changes in camera settings and particle velocities require different times between two PIV frames. For this purpose, the DaVis software allows to check the average particle displacement and adjust the timing for each experiment. The aim is to obtain an adequate number of the same particles present in both images, while at the same time the particles are displaced for about 8 pixels, as mentioned above.

Every experiment is performed three times, recording three sets of 200 pairs of images. During post-processing of the experimental

data, the images are split into a large number of interrogation windows. The latter allows calculating a particle displacement vector for each window with the help of signal processing and cross-correlation techniques. For the smallest particles used in the present study (1 and 1.5 mm diameter), two-pass processing with an initial interrogation window size of 64×64 and 98×98 pixels with no overlapping, and a second-pass window size of 32×32 pixels is used. For the largest particles (2 mm diameter), two-pass processing with a constant size interrogation window of 128×128 pixels is used. Finally, a median filter is applied in order to detect spurious vectors, while no filling for empty spaces is used.

The so-called "one quarter" rule for particle displacement was formulated to ensure enough particle pairs in high density PIV measurements, where typical interrogation windows contain few illuminated particles (6–10) in a mostly uniform background. This rule ensures that enough particle pairs can be detected in the PIV images and thus the probability that the displacement-correlation peak is larger than the random noise in the spatial cross correlation, is high (Westerweel, 1997). In the present work, typical interrogation windows contain images of closely packed particles and thus the validation of the method mostly requires ensuring that the peak of the spatial cross-correlation corresponds to real particle displacement. For this purpose the post-processing quality is validated for each experiment by using the "Image Correction and Distortion" tool available in the DaVis software. Starting from the second raw image of the PIV pair, and using the velocity field calculated, the first image is reconstructed. This reconstructed image is qualitatively compared with the captured raw image to determine the accuracy of the chosen processing parameters. For all results presented in the present work these images match very well, thus indicating the reliability of the method and the results.

Continuing the previous work, in the current experimental study three different polymers are used covering a wide range of solids densities (Table 1): High Density Poly-Ethylene (HDPE), Poly-Carbonate (PC) and Poly-VinyliDene Fluoride (PVDF). For each of these polymers, particles with different diameters are manufactured by Gala Industries® thus covering a range of particle sizes as well. The particle size distribution is analyzed using a Malvern® Mastersizer S, from which the area-weighted average particle diameter is calculated. The distributions are narrow, as shown in Table 1. The particles all belong to the Geldart-D Group when operating in the gravitational field. A wide range of gas injection velocities and solids capacities were used during the experiments to evaluate their effect on the performance of the GSVR. Further increase of the gas injection velocity is not possible due to the blower specifications. In the present study, a constant slot thickness size, i.e. 2 mm, is used and the influence of gas injection velocity is tested by increasing the gas flow rate. The maximum solids capacity is the amount of solids that can be withheld in the GSVR under given operating conditions. When additional solids are fed, they are entrained by the air, leaving the vortex chamber through the central outlet. All experimental operating conditions are gathered in Table 1. An averaged value of the bed height, h, is obtained visually using a set of rulers positioned on the GSVR end-wall. An averaged solids fraction, ε_s, and void fraction, ε, for the bed are calculated, based on the visually measured averaged bed height and the bed mass W_S.

$$\varepsilon_s = 1 - \varepsilon = \frac{W_S}{\rho_s \pi((D_R^2/4) - ((D_R/2) - h)^2) L_R} \quad (1)$$

where ρ_s is the solids density, D_R the GSVR diameter and L_R the GSVR length.

3. Results and discussion

As discussed by Kovacevic et al. (2014) the particle diameter, solids density and gas injection velocity have a significant influence on the stability of a rotating fluidized bed. The results presented here are limited to stable and semi-stable bed behavior, as defined by Kovacevic et al. (2014). Snapshots and Videos will show how the behavior of a (semi-)stable bed of different particle diameters or solid densities changes from a very dense and smoothly rotating bed to a bubbling fluidized bed. It should be noted that all presented measurements and pictures are recorded slightly left from the bottom of the reactor, which is mounted with a horizontal axis of rotation and operating with a counterclockwise flow. To allow for a better positioning of the presented images with respect to the GSVR geometry and the flow, the location of the recorded images is schematically shown in Fig. 1(b).

The three snapshots shown in Fig. 2, taken with the 2D Standard PIV, reveal the bed behavior for HDPE particles for three different particle diameters (1 mm, 1.5 mm and 2 mm) at 100 m/s gas injection velocity.

Particles of all diameters are seen to create a stable bed at these operating conditions. Fig. 2(a) shows that a bubbling fluidized bed is formed by the 1 mm diameter particles. The bubbles, the edge of the bed and the average bed height are approximately indicated with the yellow, red and blue dotted lines respectively in Fig. 2(a). The incoming air is shown to denote the flow direction. A better observation of the flow can be obtained through the corresponding Video S1 in Supplementary material. The bubbles are observed to move very fast to the edge of the bed, where they burst and entrain a limited number of particles from the edge of the bed into the freeboard of the GSVR and towards the central gas outlet. However, these particles are seen to return to the bed. As a result, the edge of the bed is not clearly defined but oscillates.

When increasing the particle diameter to 1.5 mm, Fig. 2(b), the bed is still in the bubbling regime. Although the number of gas bubbles clearly reduces, the edge of the bed still fluctuates significantly. A further increase of the particle diameter to 2 mm, Fig. 2(c), shows that the number of gas bubbles in the bed diminishes and the edge of the bed is better defined. This indicates that particles of larger diameter, that are heavier, are more difficult to entrain, as expected. At constant solids density, the bubbling behavior of the bed thus reduces with increasing particle diameter

Table 1
Operating conditions of the GSVR.

Operating conditions – primary phase (gas)						
Gas injection velocity (in inlet slots)			m/s	55, 70, 85, 100, 110		
Gas density (25 °C, 1 atm)			kg/m^3	1.225		
Operating conditions – secondary phase (solids)						
Solids capacity	kg	2, 3, 4, maximum capacity				
Material		HDPE			PC	PVDF
Diameter	mm	1	1.5	2	2	2
Particle size distribution	mm	0.9 ± 0.3	1.4 ± 0.4	1.8 ± 0.5	1.9 ± 0.6	1.9 ± 0.6
Density	kg/m^3	950	950	950	1240	1780

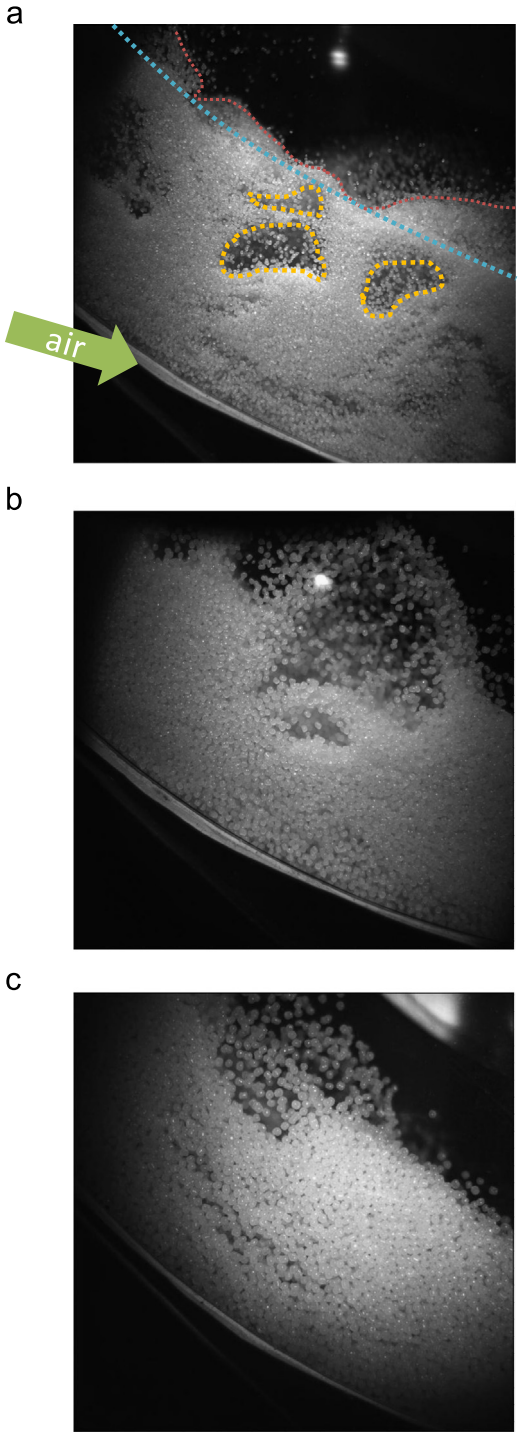

Fig. 2. Bed behavior with changing particle diameter, HDPE (ρ_s=950 kg/m^3); $v_{g,inj}$=100 m/s, maximum solids capacity. (a) d_p=1 mm; (b) d_p=1.5 mm; and (c) d_p=2 mm.

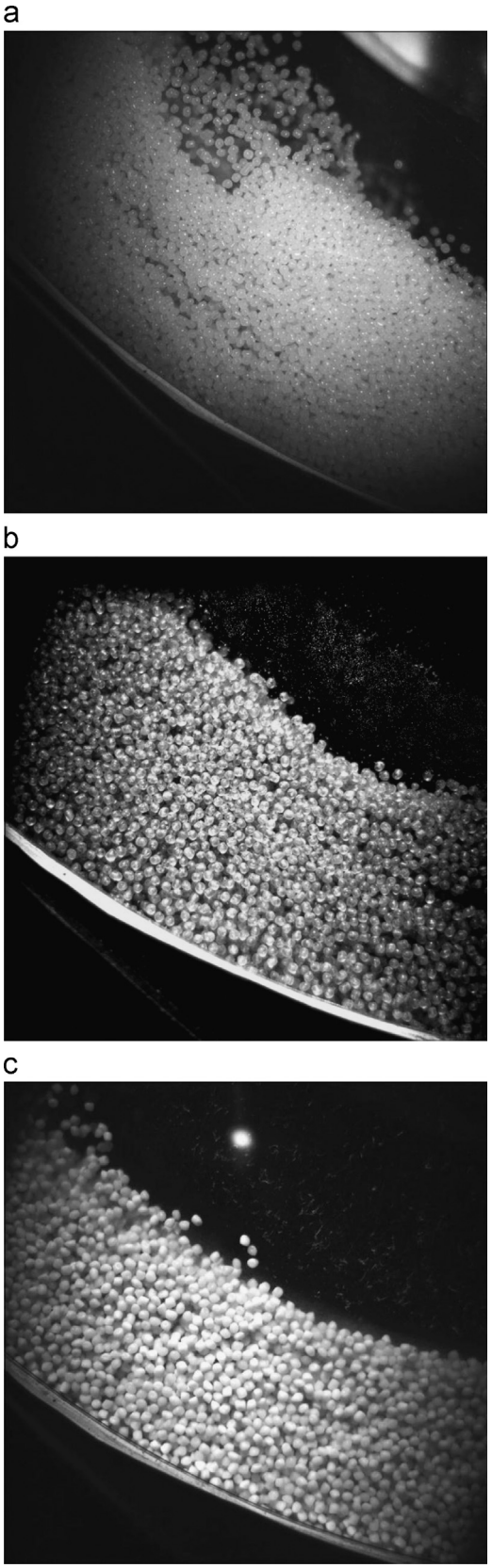

Fig. 3. Bed behavior with changing particle density. (a) HDPE (ρ_s=950 kg/m^3); (b) PC (ρ_s=1240 kg/m^3); and (c) PVDF (ρ_s=1780 kg/m^3). d_p=2 mm, $v_{g,inj}$=100 m/s, maximum solids capacity.

shown in more detail in Supplementary material, Videos S1, S2 and S3.

Supplementary material related to this article can be found online at http://dx.doi.org/10.1016/j.ces.2014.10.020.

In Fig. 3 the bed behavior for 2 mm diameter particles with increasing solids density is presented. The gas injection velocity is set at 100 m/s. In Fig. 3(a) the bed behavior of 2 mm diameter HDPE (950 kg/m^3) particles is depicted. The bed behavior was already discussed in Fig. 2(c) and shown in Video S3. Although gas bubbles appear from time to time, the edge of the bed is quite clearly defined. When feeding PC particles of higher solids density (1240 kg/m^3) gas bubbles almost disappear, Fig. 3(b) and Video S4.

Although the particles (visually) seem to rotate as a closely packed bed, the average solids fraction value is in all cases significantly lower than 0.6, the value corresponding to closely packed bed conditions. Note that the photos in the figures are just snapshots. Averaged over time, oscillations of the edge of the bed are rather limited and the edge of bed becomes more distinct. When the solids density further increases, by using PVDF (1780 kg/m^3) particles, the bed develops into a smoothly rotating dense-but still fluidized-bed, Fig. 3(c) and Video S5. The bed height remains nearly constant as a function of time and the edge of the bed becomes sharp. The bed behavior of 2 mm diameter particles with changing solids density can be studied in Supplementary material, Videos S3, S4 and S5. It can be concluded from the recordings that the increase of particle density suppresses bubbling.

Supplementary material related to this article can be found online at http://dx.doi.org/10.1016/j.ces.2014.10.020.

In Fig. 4 the bed behavior for 1.5 mm diameter HDPE (950 kg/m^3) particles is captured for different solids capacities. The gas injection velocity is set at 110 m/s. In Fig. 4(a) the 1.5 mm diameter HDPE bed behavior with a 3 kg solids capacity is shown. A smoothly rotating, dense bed is observed. Bubbling is limited and the edge of the bed is very sharp. Solids fraction measurements show that the bed is not closely packed, but in all cases the solids fraction is less than 0.45. When increasing the mass of solids in the reactor chamber to 4 kg, Fig. 4(b), the number of bubbles in the bed is seen to increase. A major part of the bed is still dense and smoothly rotating, but when bubbles reach the edge of the bed they break, dragging particles in the freeboard (as discussed above). The bed edge starts to fluctuate and is less defined. For an additional increase of the particle mass to the maximum solids capacity, 5.4 kg under the given operating conditions, Fig. 4(c), the bubbles become more prominent. The edge of bed is no longer clearly defined as already discussed for the snapshot shown in Fig. 2(a). The recordings clearly show that a decrease of solids capacity suppresses bubbling. It should be noted that in all cases studied in this work, the solids capacity used is higher than the minimum solids capacity of the GSVR (Ekatpure et al., 2011), for which slugging and channeling is observed.

3.1. Azimuthal particle velocity measurements

In this section, the azimuthal particle velocities measured slightly left of the bottom of the GSVR, in 12×12 cm^2 field of view (Fig. 1), obtained with 2D Standard PIV measurements are presented. Moreover, the influence of solids density, particle diameter and gas injection velocity on the azimuthal particle velocity component will be studied. The radial and axial particle velocity components are negligible while the azimuthal component is dominant and is responsible for the centrifugal force of the bed.

In Fig. 5(a), a single raw image is shown. Processing that image results in the particle velocity field shown in Fig. 5(b). Fig. 5(c) presents the corresponding particle velocity field obtained when averaging 200 images. From the post-processed images it is decided that time-averaged azimuthal velocities do not change significantly with the azimuthal coordinate in the PIV images due to the limited variation of the azimuthal coordinate. Therefore, time-averaged azimuthal particle velocities along a single azimuthal angle ($\theta = -35^\circ$) will be presented and discussed in the following Figures. The position of this azimuthal angle is marked in Figs. 1(b) and 5.

To assess the influence of the solids density ρ_s on the azimuthal particle velocity, experiments with 2 mm diameter particles of HDPE (950 kg/m^3) and PC (1240 kg/m^3) are analyzed. The gas injection velocity is 100 m/s. The azimuthal particle velocity profiles across a rotating bed are presented in Fig. 6. The

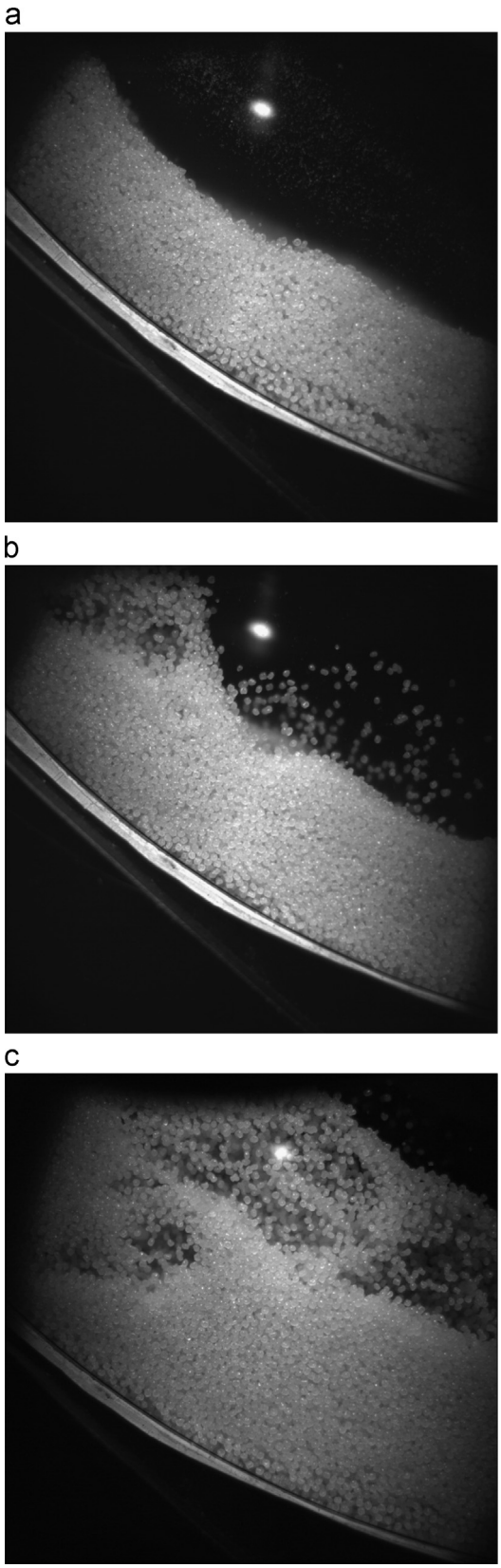

Fig. 4. Bed behavior with increasing solids capacity. (a) 3 kg; (b) 4 kg; and (c) maximum capacity (5.4 kg). HDPE (ρ_s=950 kg/ m^3), d_p=1.5 mm, $v_{g,inj}$=110 m/s.

measurements are done at the maximum solids capacity, 5.5 kg and 5.8 kg, respectively. Even though increasing the solids density should result in higher maximum capacity (Kovacevic et al., 2014), in

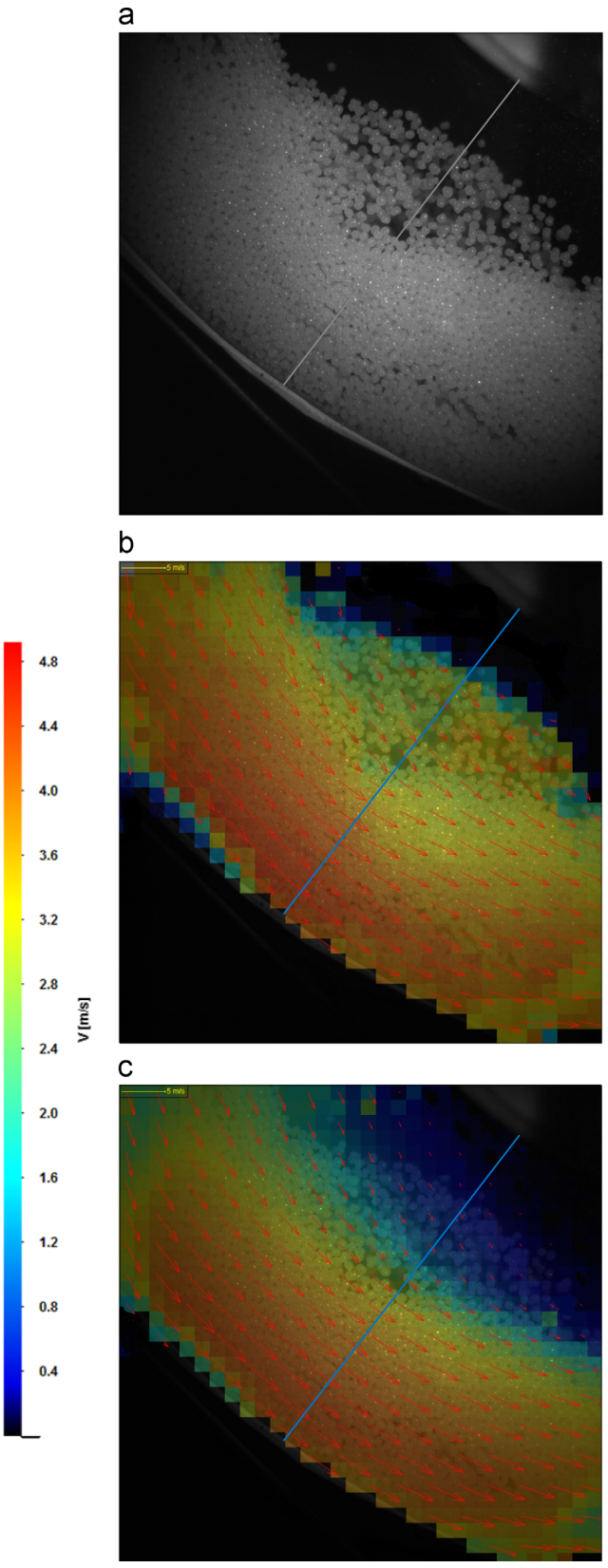

Fig. 5. Velocity vector field obtained with a 2D Standard PIV for HDPE (ρ_s=950 kg/m^3), d_p=2 mm, $v_{g,inj}$=55 m/s, maximum capacity: (a) raw image; (b) vector field of one processed image; and (c) averaged velocity field of 200 processed images.

this case the maximum capacity is almost the same. This is due to the difference in fluidization behavior, as PC particles create a semi-stable bed with limited bubbles and intense fall-out at the top of the GSVR

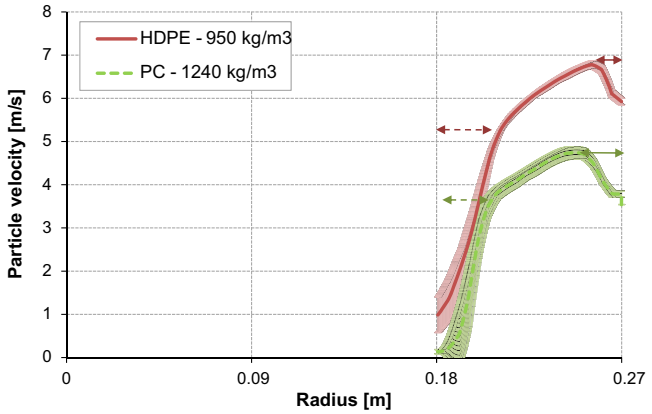

Fig. 6. Azimuthal particle velocity across a rotating bed for HDPE (ρ_s=950 kg/m^3) and PC (ρ_s=1240 kg/m^3), d_p=2 mm and $v_{g,inj}$=100 m/s, maximum solids capacity. The circumferential wall is located at r=0.27 m. Faded background represents the $\pm$ standard deviation based on three repeated experiments. Solid arrows indicate the first layer of the bed close to the gas inlet slots where the particles accelerate. Dashed arrows indicate the extent of the edge of the bed.

(Kovacevic et al., 2014), while the HDPE particles form a stable bed where intense bubbling is observed.

The curves in Fig. 6 are representative for rotating beds with a limited entrainment of particles over the edge of the bed (Fig. 3 (a) and (b)). Close to the circumferential wall (r=0.27 m), where the gas is entering in the reactor chamber through the tangential inlet slots, the contact between the gas and particles is poor. The momentum transfer from gas to particles is limited. As a result, the azimuthal particle velocity close to the circumferential wall is low and increases as the radius decreases. The momentum input is constant in both cases shown, but heavier particles are less accelerated. Thus the azimuthal velocity of heavier particles in the first layer of the bed, shown by the solid arrows in Fig. 6, is lower. It should be noted that this cannot be visually observed. As gas and particles further interact, particle momentum increases, resulting in a rising azimuthal particle velocity. A maximum in the particle azimuthal velocity is observed slightly downstream the circumferential wall. For lighter material this maximum is observed closer to the wall, due to faster acceleration. Even though the momentum input is constant for both cases, lower azimuthal velocities are recorded for PC particles. This is not expected given that the bed contains the same total mass in both cases. It should be attributed to the interaction between the two phases, the different fluidization behavior, as well as the stability of the bed formed, considering that there are qualitative differences observed, as mentioned previously. Remark also that the solids fraction values measured vary significantly between HDPE and PC beds, i.e. from 0.43 to 0.32 respectively. Downstream of the point of maximum azimuthal velocity, the momentum transfer between the phases decreases and the azimuthal particle velocity slightly drops due to friction. The position where the slope of the particle velocity profiles significantly changes corresponds to the edge of the bed and the beginning of the freeboard. The edge of the bed for both cases shown in Fig. 6 can be considered rather clearly defined, at about r=0.20 m and r=0.21 m for PC and HDPE respectively.

In Fig. 7 the azimuthal particle velocity profiles are presented for HDPE particles of different diameters (1 mm, 1.5 mm, 2 mm). The gas injection velocity is 100 m/s. The azimuthal particle velocity decreases with increasing particle diameter. As the gas injection velocity is constant, the momentum input in the reactor chamber is constant for all experiments. The maximum solids capacity increases with increasing particle diameter (Kovacevic et al., 2014), while the azimuthal velocity decreases with increasing diameter. As discussed in Fig. 6, the position of the maximum

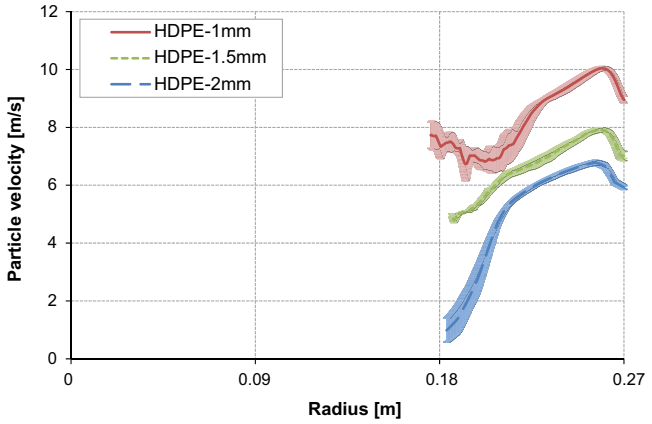

Fig. 7. Azimuthal particle velocity across a rotating solids bed of HDPE (ρ_s=950 kg/m^3) particles of diameter,:d_p: 1 mm; 1.5 mm and 2 mm at $v_{g,inj}$=100 m/s and maximum solids capacity. Faded background represents the ± standard deviation based on three repeated experiments.

shifts and the thickness of the first layer increases as the particle density increases. Remark that in Fig. 6, the mass of the particles increases due to increasing solids density, while in Fig. 7 it increases due to increasing particle diameter. As discussed in Fig. 2, with decreasing particle diameter, the bubbling behavior of a bed of HDPE particles becomes more prominent. Defining the edge of the bed becomes difficult due to the eruption of gas bubbles resulting in particle entrainment into the freeboard. The velocity of the entrained particles is measured by the PIV as well. The eruption of gas bubbles at the edge of the bed and the particle entrainment result in strong particle velocity fluctuations, as observed in Fig. 7 for 0.18 m < r < 0.21 m. Thus determining the edge of the bed from Fig. 7 becomes more difficult. For larger particles bubbling, and thus particle velocity fluctuations close to the edge of the bed, diminishes. The edge of the bed can be more clearly defined.

By increasing the gas injection velocity and thus the momentum input, while keeping the particle density and diameter constant, the azimuthal bed velocity is expected to increase. The latter behavior is confirmed in Fig. 8, where the maximum azimuthal particle velocity for all recorded operating conditions is presented as a function of the gas injection velocity. As previously discussed the maximum values are recorded slightly downstream of the circumferential wall. The increase of the maximum azimuthal particle velocity with increasing gas injection velocity is almost linear, for all particles studied and at different solids capacities. Furthermore, for lower gas injection velocities more intense fluctuations of the edge of the bed are recorded (not shown). The maximum azimuthal particle velocity is clearly affected by the particle diameter and the solids density (Fig. 8 (a)), as discussed previously (Figs. 6 and 7). It is affected by the solids capacity as well (Fig. 8(b)), as higher solids capacities result in lower particle velocities. This is in agreement with the velocity measurements performed by Anderson et al. (1972).

Fig. 9 reveals how the azimuthal particle velocity profile changes with increasing solids capacity. Experiments with HDPE particles of 1.5 mm diameter at different solids capacities, 3 kg, 4 kg and maximum capacity (5.4 kg), are performed at a gas injection velocity of 110 m/s. As expected, with increasing solids capacity, at constant gas injection velocity, that is constant momentum input, the azimuthal particle velocity in the main part of the bed will decrease. The main part of the bed extends from the circumferential wall up to the point the edge starts and is indicated by arrows in Fig. 9. The particle velocity at the edge of the bed should not be considered in this case, as the size and

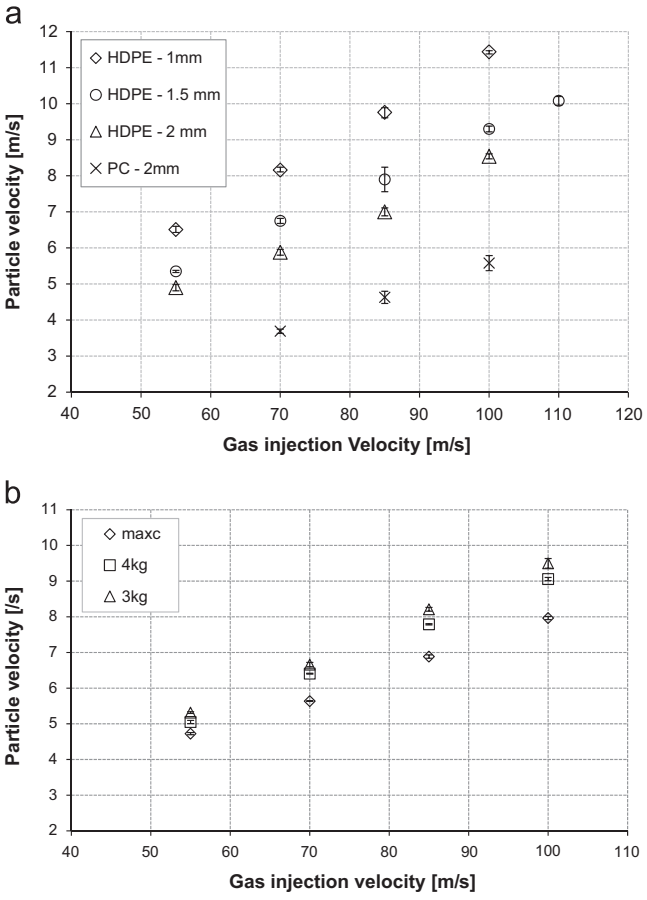

Fig. 8. Maximum azimuthal particle velocities with changing gas injection velocity for (a) 2 kg solids capacity and (b) HDPE 1.5 mm particles. Error bars represent ± standard deviation based on three repeated experiments.

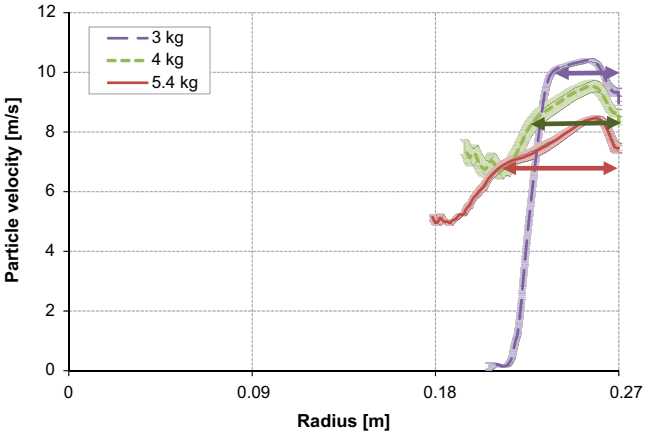

Fig. 9. Azimuthal particle velocity profiles across the rotating solids bed for different solids capacities: 3 kg; 4 kg; max capacity (5.4 kg). HDPE (d_p=950 kg/m^3); d_p=1.5 mm; at $v_{g,inj}$=110 m/s. Faded background represents the ± standard deviation based on three repeated experiments. Arrows indicate the location of the main part of the bed.

velocity of the bubbles can affect the velocity of the particles that are entrained during bubble eruption, as explained. When increasing the solids capacity, that is the number of particles in the bed, the gas momentum needs to be imparted over more particles, resulting in a decreasing azimuthal particle velocity. At low solids capacity the azimuthal particle velocity is high and the centrifugal force largely exceeds the drag force. As a result, the bed in the GSVR is a smoothly rotating dense bed with a clearly defined sharp

edge, as already observed and discussed in Fig. 4(a). As the solids capacity increases, the bed becomes less dense and finally turns into a bubbling fluidized bed (for 1.5 mm HDPE particles, Fig. 4(c)). The drag force at the edge of the bed now exceeds or is comparable to the centrifugal force. Particles are entrained into the freeboard of the reactor chamber. As a consequence, the edge of the bed is difficult to define, as discussed in Fig. 2(a). Remark that at even lower solids capacity the nearly flat part of the profile finally disappears. At a solids capacity of about 2 kg (not shown), the azimuthal particle velocity reaches a maximum value which almost immediately drops to zero, as the bed is very thin.

3.2. Minimum fluidization velocity and mapping

As mentioned by several researchers in the past (Chen, 1987; Fan et al., 1985; Kao et al., 1987; Zhu et al., 2003) the minimum fluidization velocity in rotating fluidized beds can be calculated based on the radial momentum balance. The drag force and centrifugal force are the dominating contributions (Kao et al., 1987; Zhu et al., 2003). Note that the superficial radial gas velocity is not constant but increases as the radius decreases, due to the decrease of the available flow area. This implies that the radial drag force increases with decreasing radius. For a packed bed the radial drag force per unit volume, $F_{D,r}$, can be calculated from the Ergun equation

$$F_{D,r} = 150\frac{\mu_g(1-\varepsilon)^2}{\varepsilon^3 d_p^2}v_{g,r} + 1.75\frac{(1-\varepsilon)\rho_g}{\varepsilon^3 d_p}v_{g,r}^2 = \varphi_1 v_{g,r} + \varphi_2 v_{g,r}^2 \quad (2)$$

where $v_{g,r}$ is the gas radial superficial velocity, μ_g is the gas viscosity, ε is the void fraction of the bed and ρ_g is the gas density. μ_g and ρ_g are considered for ambient conditions, that is 1.8×10^{-5} Pa·s and 1.225 kg/m^3 respectively. Note that ε is radius-dependent due to the layer-by-layer fluidization. The centrifugal force per unit volume, $F_{c,r}$, is proportional to the radial coordinate assuming the angular velocity ω remains constant throughout the bed

$$F_{c,r} = \rho_s(1-\varepsilon)r\omega^2 \quad (3)$$

Once the drag force balances the centrifugal force of the packed bed, fluidization is initiated. Accounting for the above discussion, both forces will first balance at the edge of the bed. As the gas injection velocity increases, fluidization is observed inside the bed. Finally, fluidization reaches the circumferential wall of the reactor chamber and the complete bed is fluidized. This is the layer-by-layer fluidization as described in literature (Chen, 1987; Kao et al., 1987; Zhu et al., 2003). The minimum fluidization velocity is a function of the radial position in the bed that can be calculated by equating the drag force, Eq. (2), and the centrifugal force, Eq. (3), and solving for the gas radial velocity

$$v_{mf,r} = \frac{\sqrt{\varphi_1^2 - 4\varphi_2\rho_s(1-\varepsilon)r\omega^2} - \varphi_1}{2\varphi_2} \quad (4)$$

As there is no measurement of the local bed void fractions, the average void fraction calculated from Eq. (1) has been used in all calculations. For the GSVR the angular velocity ω is estimated based on the maximum azimuthal particle velocity, v_{θ,r_m}, obtained by the PIV measurements

$$\omega = \frac{v_{\theta,r_m}}{r_m} \quad (5)$$

Fluidization starts at radial gas velocity $v_{mf,i}$, which is the minimum fluidization velocity at the edge of the bed, while the bed is completely fluidized at $v_{mf,cr}$ the minimum fluidization velocity at the circumferential wall of the reactor chamber. The latter is referred to as the critical minimum fluidization velocity. The minimum fluidization velocities at the inner edge of the bed and at the circumferential wall are presented in Fig. 10 in terms of a dimensionless particle size (or modified Archimedes number),

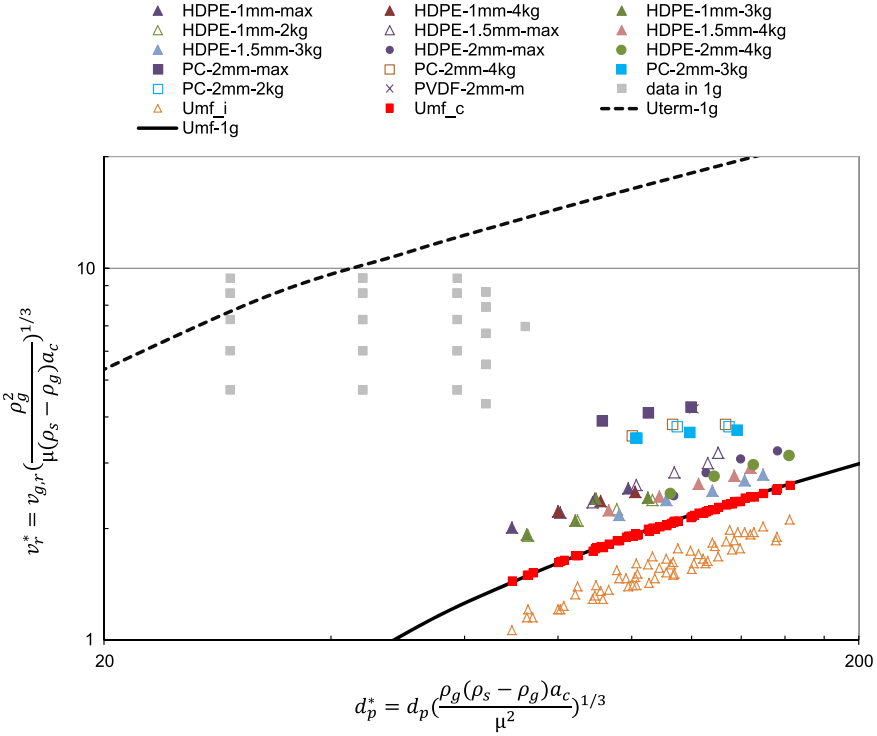

Fig. 10. Indicative representation of the GSVR data in terms of dimensionless particle diameter and radial velocity. The lines correspond to the minimum fluidization velocity ($U_{mf}-1$g, solid line), and the terminal velocity ($U_{term}-1$g, dashed line) for gravitational fluidized beds. '1g' refers to the data calculated using the gravitational acceleration instead of the centrifugal acceleration. U_{mf}_c and U_{mf}_i correspond to the dimensionless minimum fluidization velocities calculated at the circumferential wall and at the edge of the bed respectively.

d_p^*, and a dimensionless gas velocity, v_r^*, as it is common practice for conventional fluidized beds (Grace, 1986).

$$d_p^* = d_p \left(\frac{\rho_g \left(\rho_s - \rho_g\right) a_c}{\mu_g^2} \right)^{1/3} \tag{6}$$

$$v_r^* = v_{g,r} \left(\frac{\rho_g^2}{\mu_g \left(\rho_s - \rho_g\right) a_c} \right)^{1/3} \tag{7}$$

$$a_c = \frac{v_{\theta,r_m}^2}{r_m} \tag{8}$$

In a centrifugal field these dimensionless values are calculated using the centrifugal acceleration, a_c, instead of the gravitational acceleration as used for conventional fluidized beds. The dimensionless velocity and the corresponding modified Archimedes number for all operating conditions studied have been calculated and the results are presented in Fig. 10. The line showing the minimum fluidization velocity for conventional (gravitational) fluidized beds is plotted for reference in Fig. 10. For all experiments in the present work the superficial radial gas velocity is found to be higher than the critical minimum fluidization velocity $v_{mf,cr}$, implying that the bed is always fully fluidized. For reasons of comparison, the dimensionless values for the experiments are calculated using the gravitational acceleration instead of the centrifugal acceleration. They are also presented in Fig. 10 (gray squares). A shift towards higher Archimedes numbers and lower dimensionless velocities v_r^* in a centrifugal field, as compared to the gravitational field, is clearly observed. As discussed in detail previously, limited to extensive bubbling behavior is observed for most of the experimental conditions. This is verified in Fig. 10 which is however based on the flow regime map constructed for gravitational fluidized beds (see e.g. Grace, 1986), given the lack of a more appropriate flow regime diagram for GSVRs. It should be noted though, that contrary to gravitational fluidized beds, spouting or complete penetration of the bed by a jet of gas, as in spouted beds, has not been observed in the GSVR, even though the bubbles recorded by the PIV are sometimes quite thin and elongated.

3.3. Solids velocity at maximum solids capacity conditions

When the GSVR is operating at maximum solids capacity conditions, adding a small amount of particles will result in particle entrainment by the gas, removing an equivalent quantity of particles from the GSVR via the central gas outlet. The entrainment of particles takes place at the top left corner of the GSVR, due to the effect of gravity in combination with the geometrical configuration of the set-up in the present study, i.e. horizontal-axis GSVR and anti-clockwise rotation of the bed, as also reported by Kovacevic et al. (2014). This implies that the radial forces acting on the particles in the edge of the bed at the top of the GSVR are practically balanced. On the one hand, feeding particles will result in a decrease of the azimuthal particle velocity, corresponding to a decrease of the centrifugal force. On the other hand, feeding of particles will result in an increase of the bed height, corresponding to an increase of the radial superficial gas velocity at the edge of the bed, and hence an increase of the drag force. As a result, particles will be entrained by the gas and leave through the central gas outlet. Applying the radial force balance slightly left from the top of the GSVR where entrainment is first observed (Kovacevic et al., 2014), allows calculating a local particle azimuthal velocity

$$F_{c,r_i} = -F_{g,r} + F_{D,r_i} \tag{9}$$

$$F_{g,r} = \rho_s (1-\varepsilon) g \cos\theta \tag{10}$$

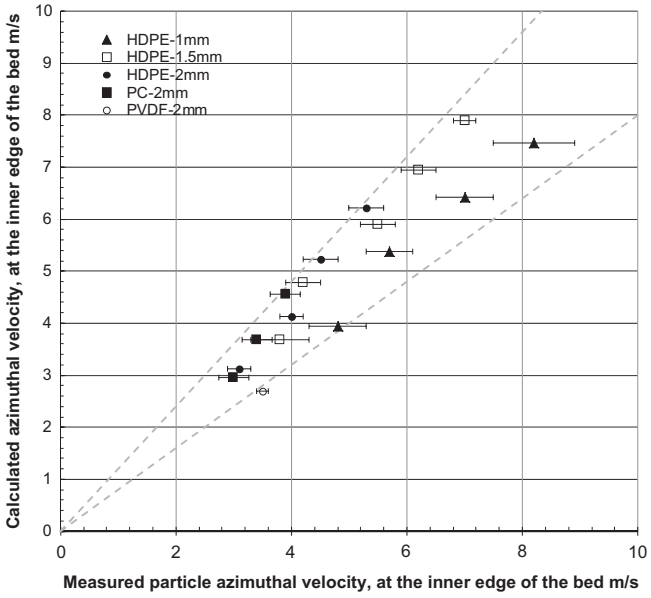

Fig. 11. Calculated azimuthal particles velocities (Eq. (11)) at the edge of the bed in the GSVR for $\theta = 180^\circ$ versus measured particle velocities. Error bars indicate the deviation from the value reported due to the difficulties in defining the bed edge as a result of its fluctuations. Dashed lines indicate $\pm 20\%$ deviation.

$$v_{s,\theta} = \sqrt{\frac{\varphi_1}{(1-\varepsilon)\rho_s} v_{g,r_m} r_m + \frac{\varphi_2}{\rho_p (1-\varepsilon)} \frac{v_{g,r_m}^2 r_m^2}{r_i} - r_i g \cos\theta} \tag{11}$$

where θ is the azimuthal coordinate, see Fig. 1, r_m is the radial position where maximum azimuthal particle velocity is measured (close to the circumferential wall, Fig. 6) and r_i is the radial coordinate of the edge of the bed. An averaged void fraction, ε, calculated based on the visually measured bed height in the top of the GSVR and the total mass of the bed is used. Even though it is shown in Fig. 5 that the azimuthal particle velocities are locally independent of the azimuthal coordinate within the frames of the PIV images, the influence of gravity becomes more prominent at the top of the reactor, and the azimuthal particle velocity varies slightly at the four quadrants of the GSVR chamber (top, bottom, left and right). However, this variation is estimated to be limited. In Fig. 11, the values for the azimuthal particle velocity slightly left from the top of the GSVR, calculated using Eq. (11), and the azimuthal particles velocity measured slightly left from the bottom of the GSVR, are compared. The comparison between experimentally determined and calculated values is satisfying, the deviations are less than 20%.

4. Conclusions

Experimental research in a pilot-scale Gas–Solid Vortex Unit is performed over a broad range of 40 different operating conditions. The influence of the gas injection velocity, the particle diameter, the solids density and solids capacity on the hydrodynamics of the fluidized bed and in particular on the azimuthal particle velocity is studied using PIV. The experiments show that the tested operating parameters have a significant influence on the bed fluidization, as well as on the azimuthal particle velocity.

The bubbling fluidized bed with fluctuations at the edge of the bed is observed to become a densely fluidized bed with a clearly defined edge, when the particle diameter increases from 1 mm to 2 mm. With increasing the particle density (from 950 kg/m^3 to 1780 kg/m^3) bubbling is suppressed. With increasing bed mass, the bed changes from densely fluidized to bubbling. The azimuthal particle velocity decreases with increasing particle diameter and

with increasing bed mass. For all studied operating conditions, the superficial gas velocities are found to be higher than the calculated critical minimum fluidization velocity for a rotating fluidized bed. Therefore, in all experiments completely fluidized beds are obtained, as verified by solids fraction estimates. The results for all operating conditions are presented in terms of dimensionless groups that are usually utilized for conventional fluidized beds. At maximum solids capacity a force balance at the inner edge of the bed and at the top of the GSVR where particles start being entrained by the gas is performed. The calculated azimuthal velocities deviate less than 20% from the measured azimuthal particle velocity at the inner edge of the bed close to the bottom of the reactor, showing that particle velocities can be well predicted.

Nomenclature

a_c	centrifugal acceleration [m/s^2]
d_p	particle diameter [m]
d_p^*	dimensionless particle size (or modified Archimedes number) [dimensionless]
D_R	GSVR diameter [m]
$F_{c,r}$	radial centrifugal force per unit volume [N/m^3]
$F_{D,r}$	radial drag force per unit volume [N/m^3]
$F_{g,r}$	radial gravitational force per unit volume [N/m^3]
h	bed height [m]
L_R	GSVR length [m]
r	radial position [m]
r_i	radial position of the inner edge of the bed [m]
r_m	radial position where maximum azimuthal particle velocity is measured [m]
$v_{g,inj}$	gas injection velocity [m/s]
$v_{g,r}$	radial superficial gas velocity [m/s]
$v_{mf,r}$	radial minimum fluidization velocity [m/s]
$v_{mf,i}$	minimum fluidization velocity at the edge of the bed [m/s]
$v_{mf,cr}$	fluidization velocity when bed is completely fluidized [m/s]
v_{θ,r_m}	maximum azimuthal particle velocity [m/s]
$v_{s,\theta}$	local azimuthal particle velocity [m/s]
v_r^*	dimensionless radial gas velocity [dimensionless]
W_S	solids capacity [kg]

Greek symbols

ε	void fraction [dimensionless]
ε_s	solids fraction [dimensionless]
θ	azimuthal coordinate [deg]
μ_g	gas dynamic viscosity [Pa·s]
ρ_g	gas density [kg/m^3]
ρ_s	solids density [kg/m^3]
φ_1	$150(1-\varepsilon)^2\mu_g/\varepsilon^3 d_p^2$, drag coefficient [kg/m^3 s]
φ_2	$1.75(1-\varepsilon)\rho_g/\varepsilon^3 d_p$, drag coefficient [kg/m^4]
ω	angular velocity [rad/s]

Acknowledgment

The authors acknowledge financial support from the “Long Term Structural Methusalem Funding by the Flemish Government” and from the European Research Council under the European Union's Seventh Framework Program FP7/2007-2013 ERC Grant agreement no. 290793.

References

Anderson, L., Hasinger, S., Turman, B., 1972. Two-component vortex flow studies of the colloid core nuclear rocket. J. Spacecr. 9, 311–317.
Chen, Y.M., 1987. Fundamentals of a centrifugal fluidized bed. AIChE J. 33, 722–728.
De Wilde, J., de Broqueville, A., 2007. Rotating fluidized beds in a static geometry: experimental proof of concept. AIChE J. 53, 793–810.
De Wilde, J., de Broqueville, A., 2008. Experimental investigation of a rotating fluidized bed in a static geometry. Powder Technol. 183, 426–435.
Dutta, A., Ekatpure, R.P., Heynderickx, G.J., de Broqueville, A., Marin, G.B., 2010. Rotating fluidized bed with a static geometry: guidelines for design and operating conditions. Chem. Eng. Sci. 65, 1678–1693.
Dvornikov, N.A., Belousov, P.P., 2011. Investigation of a fluidized bed in a vortex chamber. J. Appl. Mech. Tech. Phys. 52, 206–211.
Ekatpure, R.P., Suryawanshi, V.U., Heynderickx, G.J., de Broqueville, A., Marin, G.B., 2011. Experimental investigation of a gas–solid rotating bed reactor with static geometry. Chem. Eng. Process.: Process Intensif. 50, 77–84.
Eliaers, P., de Broqueville, A., Poortinga, A., van Hengstum, T., De Wilde, J., 2014. High-G, low-temperature coating of cohesive particles in a vortex chamber. Powder Technol. 258, 242–251.
Fan, L.T., Chang, C.C., Yu, Y.S., Takahashi, T., Tanaka, Z., 1985. Incipient fluidization condition for a centrifugal fluidized bed. AIChE J. 31, 999–1009.
Geldart, D., 1973. Types of gas fluidization. Powder Technol. 7, 285–292.
Grace, J.R., 1986. Contacting modes and behaviour classification of gas–solid and other two-phase suspensions. Can. J. Chem. Eng. 64, 353–363.
Kao, J., Pfeffer, R., Tardos, G.I., 1987. On partial fluidization in rotating fluidized beds. AIChE J. 33, 859–861.
Keane, R.D., Adrian, R.J., 1990. Optimization of particle image velocimeters. Part I: double pulsed systems. Meas. Sci. Technol. 1, 1202–1215.
Kochetov, L.M., Sazhin, B.S., Karlik, E.A., 1969. Experimental determination of the optimal ratios of structural dimension in the swirl chamber for drying granular material. Khimicheskoe i Neftyanoe Mashinostroenie 2, 10–11.
Kovacevic, J.Z., Pantzali, M.N., Heynderickx, G.J., Marin, G.B., 2014. Bed stability and maximum solids capacity in a Gas–Solid Vortex Reactor: experimental study. Chem. Eng. Sci. 106, 293–303.
Kroger, D.G., Abdelnour, G., Levy, E.K., Chen, J., 1980. Particle distibution and mixing in a centrifugal fluidized bed. In: Grace, J.R., Matsen, J.M. (Eds.), Fluidization. Plenum Press, New York, p. 453.
Kroger, D.G., Levy, E.K., 1979. Flow characteristics in packed and fluidized rotating beds. Powder Technol. 24, 9–18.
Kunii, D., Levenspiel, O., 1969. Fluidization Engineering.
Levy, E.K., Martin, N., Chen, J., 1979. Minimum fluidization and startup of a centrifugal fluidized bed, Fluidization. Cambridge University Press, Cambridge.
Nakamura, H., Watano, S., 2007. Numerical modeling of particle fluidization behavior in a rotating fluidized bed. Powder Technol. 171, 106–117.
Qian, G.H., Bágyi, I., Burdick, I.W., Pfeffer, R., Shaw, H., Stevens, J.G., 2001. Gas–solid fluidization in a centrifugal field. AIChE J. 47, 1022–1034.
Qian, G.H., Bágyi, I., Pfeffer, R., Shaw, H., Stevens, J., 1999. Particle mixing in a rotating fluidized bed: inferences about the fluidized state. AIChE J. 45, 1401–1410.
Takahashi, T., Tanaka, Z., Fan, L.T., 1984. Performance of a Rotating Fluidized Bed. J. Chem. Eng. Jpn. 17.
van Buijtenen, M.S., Börner, M., Deen, N.G., Heinrich, S., Antonyuk, S., Kuipers, J.A. M., 2011. An experimental study of the effect of collision properties on spout fluidized bed dynamics. Powder Technol. 206, 139–148.
Volchkov, E.P., Terekhov, V.I., Kaidanik, A.N., Yadykin, A.N., 1993. Aerodynamics and heat and mass transfer of fluidized particle beds in vortex chambers. Heat Transf. Eng. 14, 36–47.
Westerweel, J., 1997. Fundamentals of digital particle image velocimetry. Meas. Sci. Tech. 8, 1379–1392.
Zhu, C., Lin, C.H., Qian, G.H., Pfeffer, R., 2003. Modeling of the pressure drop and flow field in a rotating fluidized bed. Chem. Eng. Commun. 190, 1132–1154.